Proton irradiation induced GaAs solar cell performance degradation simulations using a physics-based model

Solar Energy Materials & Solar Cells 223 (2021) 110971

Contents lists available at ScienceDirect

Solar Energy Materials and Solar Cells

journal homepage: http://www.elsevier.com/locate/solmat

Proton irradiation induced GaAs solar cell performance degradation simulations using a physics-based model

Natasha Gruginskie [a,*], Federica Cappelluti [b], Maarten van Eerden [a], Gerard Bauhuis [a], Peter Mulder [a], Elias Vlieg [a], John Schermer [a]

[a] Radboud University, Institute for Molecules and Materials, Applied Materials Science, Heyendaalseweg 135, 6525 AJ, Nijmegen, the Netherlands
[b] Politecnico di Torino, Department of Electronics and Telecommunications, Corso Duca degli Abruzzi 24, 10129, Torino, Italy

ARTICLE INFO

Keywords:
GaAs solar cells
Thin-film solar cells
Space application
Proton irradiation

ABSTRACT

In this study a recently developed physics-based model to describe the performance degradation of GaAs solar cells upon electron irradiation is applied to analyze the effects of proton irradiation. For this purpose GaAs solar cells with significantly different architectures are subjected to a range of proton irradiation fluences up to 5×10^{12} H^+/cm^2. The resulting $J-V$ and EQE characteristics of the cells are measured and compared with the simulations from the model. The model requires individual degradation constants for the SRH lifetimes and the surface recombination velocities as an input. In this study these constants were obtained from the recently determined associated constants for electron irradiation using the particles non-ionizing energy loss (NIEL) values for conversion. The good fit between the simulated and experimentally obtained results demonstrate that this is a valid approach. Moreover, it suggests that the physics based model allows for a good prediction of GaAs cell performance under particle irradiation of any kind independent of the particular cell architecture as long as the layer thicknesses and doping levels are known. In addition the applied proton irradiation levels in this study were not found to induce additional Cu-related degradation in the investigated thin-film cells, indicating that the use of copper foil as a convenient carrier and rear contact does not require reconsideration for thin-film cells intended for space applications.

1. Introduction

The standard configuration of space solar power systems is based on triple junction III-V solar cells on a Ge substrate, that acts as a bottom sub-cell, but also provides mechanical structure and a barrier between the solar cell structure and the metal from the contacts. Devices with the thin-film architecture, on the other hand, are becoming increasingly relevant for space application studies, due to its reduced weight, flexibility [1–4] and possibility of wafer reuse [5–7], which would result in a significant reduction of costs to the system. An important point of concern for the application of thin-film devices in space, however, is the application of a copper foil as a conductive carrier to the back of the cells. Copper is known to be a fast diffuser in many semiconductors, and upon the challenging conditions of space, it may be harmful to the solar cells' performances [8,9].

Currently, most of the space solar power applications are directed towards communication satellites operating in Geostationary Earth Orbits (GEO) or in satellite constellations in Low Earth Orbits (LEO) [10]. However, new advances in satellite technology, such as elliptical orbits that partially operate in the vicinity of the Van Allen radiation belt, require the understanding of solar cell degradation upon higher levels of radiation exposure [11]. Electron irradiation is the most commonly studied characterization method to replicate cell performance under irradiation damage in the space environment [12–18]. Using this method, a pre-defined equivalent irradiation dose of 1-MeV electrons is used to simulate the displacement damage from electrons, protons, ions and neutrons of different energies throughout the entire mission. The equivalent fluence usually associated to GEO missions is achieved with 1×10^{15} 1-MeV electrons/cm^2, while 5 to 10 times lower doses are required for the simulation of LEO missions. The solar cells degradation constants for performance prediction available in literature, however, differ significantly [11,19,20]. Commonly, degradation is described in terms of experimentally determined parameter remaining factors which are valid for one particular cell architecture rather than for

* Corresponding author.
E-mail address: n.gruginskie@science.ru.nl (N. Gruginskie).

https://doi.org/10.1016/j.solmat.2021.110971
Received 8 September 2020; Received in revised form 1 December 2020; Accepted 7 January 2021
Available online 25 January 2021

the applied absorber material in general [21].

In a recent study [22], a combined experimental and theoretical analysis of the performance of GaAs solar cells with multiple architectures subjected to electron irradiation fluences equivalent to GEO missions is reported, and a consistent physical model for cell performance simulations (CPS) is proposed. An important finding from this modeling study is that, besides the increase in Shockley-Read-Hall (SRH) recombination, which reduces the minority carriers SRH lifetimes, the electron irradiation strongly affects the quality of hetero-interfaces, characterized by a linear increase in the interface recombination velocity ($S_{p(n)}$). Therefore, in addition to the SRH lifetime degradation constant ($K_{\tau p(n)}$), the model considers a linear increase in $S_{p(n)}$, and an interface recombination velocity degradation constant ($K_{Sp(n)}$) is also introduced. As a result from the CPS model fit, a coherent set of material-dependent damage constants is derived. Furthermore, this study showed that exposure to electron irradiation does not introduce additional defects to devices with the thin-film architecture, which have a Cu-foil applied as a conductive carrier. In fact, a thin-film solar cell with a shallow junction geometry showed the highest end-of-life (EOL) performance, with an efficiency equivalent to 82% of its initial value. But even though the copper was shown to comply well with the incidence of electrons, it is not known whether the incidence of different charged particles will have adverse effects to the metal-semiconductor interface, applied in direct contact to the epi-structures in this architecture.

In the present study, the previously developed CPS model is further validated for 1-MeV proton irradiation, and includes more harmful particle fluences than the equivalent to the standard GEO mission (up to 5×10^{12} 1-MeV H^+/cm^2). Proton irradiation is a less used characterization method, and the equivalent doses are not as well defined. It has been established that the degradation of the solar cells short circuit current density (J_{sc}) upon irradiation depends primarily on the fluence, while the impact of radiation on other cell parameters such as the non-radiative recombination in the space charge region and the V_{oc} is dependent on the particle type. As compared to electrons, protons have shown to cause relatively higher damage in GaAs solar cells V_{oc} and have a very irregular damage profile for lower energy particles [23,24].

A broad variation of cell architectures is applied in order to isolate the radiation damage to the hetero-interfaces from effects in the bulk of the absorber. These include devices with different junction depths (i.e. shallow and deep-junction devices) as well as cells with and without their native substrate included in the final device structure (i.e. substrate-based and thin-film cells). Moreover, the comparison between substrate-based and thin-film solar cells with otherwise identical structures allows the identification of any possible copper-related defects resultant from proton irradiation. The direct conversion of the previously reported electron irradiation degradation constants, based on the particle equivalent displacement damage dose (DDD), resulted in a good representation of the experimentally obtained dark and illuminated $J-V$ and external quantum efficiency (EQE) curves. Furthermore, an earlier reported voltage-dependency of the photocurrent [11] is seen in the irradiated cells.

2. Methods

All solar cells used in this study were grown by low-pressure MOCVD on 2 inch diameter GaAs wafers with (1 0 0) 2° off to (1 1 0) orientation. The structures consist of solar cells with either a thin *n*-doped emitter and a thick *p*-doped base, here called shallow junction (SJ) geometry, or a thick *n*-doped emitter and a thin *p*-doped base, here called deep junction (DJ) geometry. In order to evaluate the effect of irradiation on solar cells with reduced thickness, thinner DJ devices were also produced. Schematic depictions of the studied cell structures are shown in Fig. 1a–c, indicating the cells active layers thickness and acceptor and donor doping densities (N_A and N_D). Additionally, all structures have a 20 nm AlInP window and 100 nm InGaP back surface field (BSF) on the top and bottom of the active layers. The top most layer in all cells consists of a 300 nm *n*-GaAs contact, which provides low resistance ohmic contact.

The cells were processed either in the substrate-based form (SB) or into thin-film (TF) devices. For the thin-film solar cells, the first grown layer consists of an etch-stop AlGaInP layer, in order to limit the etching of the wafer, followed by a *p*-AlGaAs contact layer. The wafer was

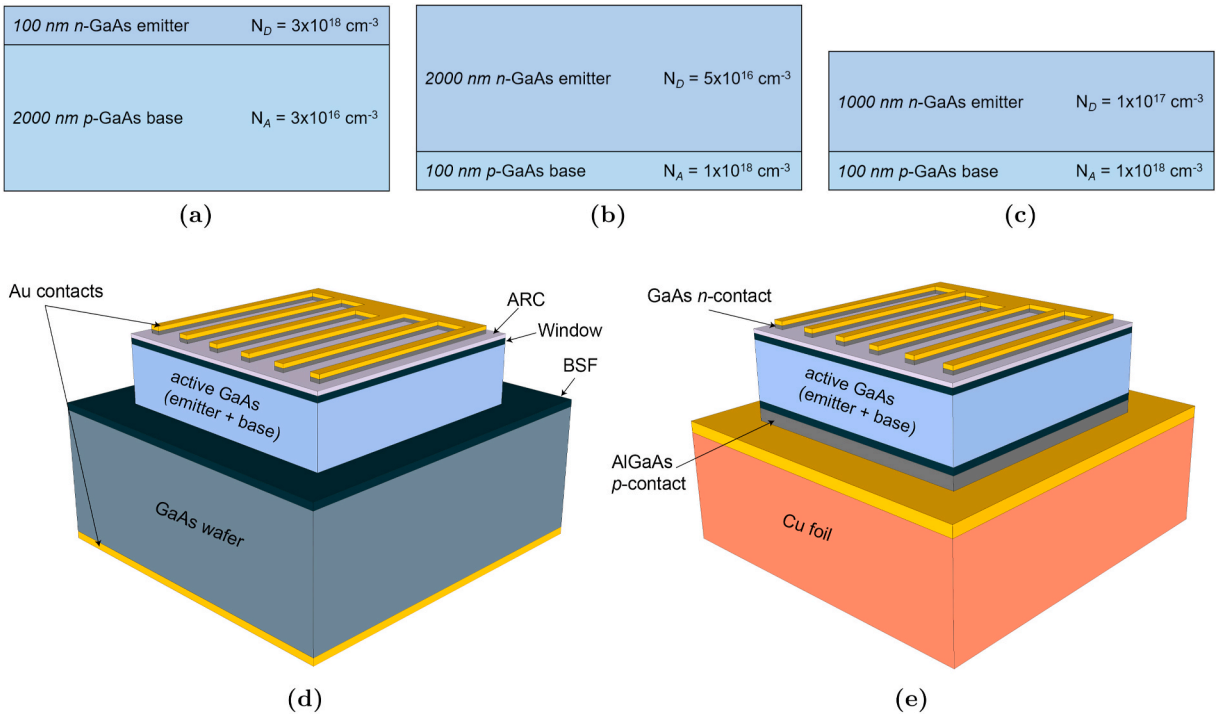

Fig. 1. Schematic depiction of a) the shallow junction, b) the deep junction and c) the thinner deep junction active layers thicknesses and acceptor and donor doping densities (N_A and N_D), and a representation of the solar cell structures processed into d) substrate based (SB) and e) thin-film (TF) devices.

removed with an aqueous citric acid and hydrogen peroxide solution (5:1 in volume) and the etch-stop layer was removed in HCl 37%. This simplified chemical etching procedure is more time-efficient and has a better yield than the more elaborative epitaxial lift-off (ELO) method, both important aspects, considering the large amount of samples required for the irradiation tests. The final thin-film devices resulting from chemically removing the substrate, however, do not differ in quality from cells produced by the ELO method, and therefore their resilience to radiation should be equivalent.

A 200 nm thick Au rear contact/mirror was electron-beam evaporated onto the rear side of the cell, and a copper foil that acts as a conductive foreign carrier was electroplated to the back of the cell. In the substrate-based devices, the back contact consists solely of 100 nm thick electron-beam evaporated Au.

The cells all have 200 nm thick Au electron-beam evaporated front contacts. This front grid includes a large contact pad to facilitate easy placement of electrical probes for cell measurements, resulting in a surface coverage of 16.6%. The 5×5 mm^2 individual cells were defined by a MESA etch using an ammonia:hydrogen peroxide solution for the GaAs layers and either an HBr:Br_2:H_2O solution (for the thin-film cells) or HCl 37% (for the substrate based cells) for the phosphide layers. The *n*-GaAs contact layer between the grid fingers was removed also using an ammonia:hydrogen peroxide solution. Finally, an anti-reflection coating (ARC) consisting of 44 nm ZnS and 94 nm MgF_2 was thermally evaporated on the top surface of all cells. A schematic depiction of the processed substrate based and thin-film devices is shown in Fig. 1d and e.

From each 2 inch wafer, 38 regular solar cells and 6 cells with an open grid dedicated for optical characterization were fabricated. The latter cells, instead of a grid, only have a square shaped contact frame at the outer edge of the front surface. The wafers were cleaved in quarters consisting of 11 solar cells and mounted to copper plates to be subjected to a specific radiation dose. The substrate-based cells were fixed to the plates using Kapton tape at the corners of the wafer. In this way an electrical contact between the rear contact of the cell and the copper plate is induced that allows convenient electrical probing of the cell with both probes at the front side. The thin-film devices were mounted to the copper plate using double sided tape, as their rear contact can be easily be reached from the front side at any location between the individual cells (see Fig. 2).

The samples were exposed to proton fluences of 5×10^{10}, 2×10^{11}, 5×10^{11}, 2×10^{12} and 5×10^{12} H^+/cm^2 of 1-MeV radiation, performed at the Center of Nuclear Science and Materials Science (CSNSM) of Paris-Sud University with a Van der Graaf accelerator. The used proton flux is equal to 1×10^9 H^+/cm^{2}s for the lower two doses and 1×10^{10} H^+/cm^{2}s for the higher three doses.

Illuminated $J-V$, dark $J-V$ and External Quantum Efficiency (EQE) characteristics were measured before and after exposure to radiation. Illuminated and dark $J-V$ characterization of the solar cells were performed using an ABET Technologies Sun 2000 Class AAA solar simulator set-up, equipped with a Keithley 2601B source meter, and ReRa Tracer3 software for data acquisition. The solar cells were kept at 25°C during measurement using a heating/cooling water thermostat and a Pt100 temperature sensor. The light intensity was set and corrected using an NREL calibrated reference cell before each measurement series. Because at higher voltages the series resistances cause the dark curve to bend downwards, a set of $J_{sc}-V_{oc}$ data points measured under different light intensities was used in the dark characteristics analysis, as the series resistance is excluded under these conditions [25]. EQE measurements were performed with a ReRa SpeQuest Quantum Effciency system. The system uses both a Xenon and Halogen light source to address all wavelengths present in the solar spectrum, a monochromator to generate quasi-monochromatic light and a chopper for intensity modulation. Due to shadow losses in the front grid, the EQE curves were corrected based on their J_{sc} values obtained by the analysis of the illuminated $J-V$.

The cells illuminated performances are modeled based on the 1D analytical Hovel model, including light reflection and photon recycling [26–29], as described in a previous publication [22]. The reflectance of the cells' front surface was calculated from the intended thickness of the ARC layers. Because there may be some difference between the intended and the actually deposited thickness, there is a level of uncertainty in the EQE fitting process, resulting in some deviations between the modeled and measured values. The main trends and shape of the curves are, however, modeled correctly.

The dark currents are in the first place analyzed as two diodes in parallel, which after de-embedding the possible influence of the parasitic series and shunt resistances, can be expressed as:

$$J_{dark} = J_{01}\left(e^{\frac{qV}{kT}} - 1\right) + J_{02}\left(e^{\frac{qV}{2kT}} - 1\right), \quad (1)$$

where q is the electron charge, k is the Boltzmann constant, T is the temperature and J_{01} and J_{02} are the saturation current densities at the $1kT$ and $2kT$ components of the curve, respectively. At higher voltages, the dark curve is dominated by J_{01}, which is composed by the diffusion

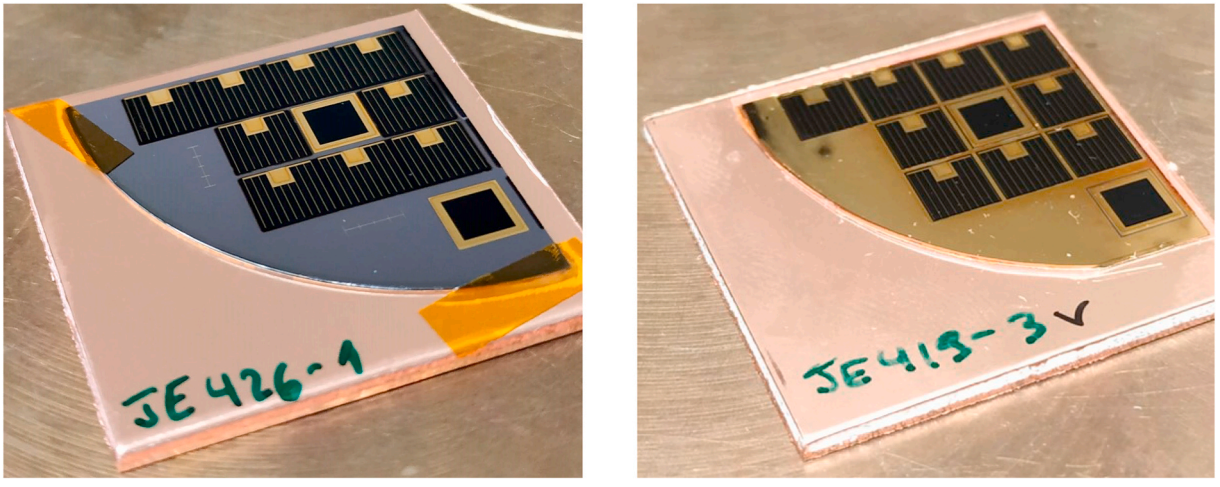

Fig. 2. Example of one quadrant of a 2-inch wafer containing multiple 5×5 mm^2 cells with the a) substrate based and b) thin-film architectures, to be subjected to a specific radiation dose. Note the large front contact pads to facilitate easy probing of the individual cells and the difference between the cells with regular grid and frame contacts for $J-V$ and EQE analysis, respectively.

and radiative recombination current densities at the quasi-neutral regions (QNR).

The J_{02} component, on the other hand, involves the non-radiative recombination that takes place predominantly in the space charge region (SCR) and the perimeter of the cell, dominating the dark current at lower voltages. The contribution from the SCR can usually be modeled according to the Shockley-Read-Hall theory [26,30], with analytical or semi-analytical formulations available under the assumption of a single mid-gap defect level [30] and for the more realistic case of multiple trap levels [21]. In the case of the solar cells in this study, however, their relatively small size results in a large contribution from perimeter recombination to the dark curves [31,32], which cannot be theoretically determined with sufficient accuracy. Therefore, while J_{01} was also calculated as reported in a previous publication [22], the J_{02} values used for simulating the cells dark and illuminated $J-V$ curves, both at BOL and upon irradiation, were experimentally obtained.

The BOL interface recombination velocities in the hetero-interfaces emitter-window (S_p) and base-BSF (S_n) were estimated by the comparison of the theoretically calculated J_{01} to the extracted values from the experimental dark curves, using equation (1). These values were then more finely adjusted by the fitting of the EQE curves.

3. Results and discussion

3.1. Solar cell performance at the beginning of life

The solar cells average illuminated $J-V$ parameters at BOL are displayed in Fig. 3, as well as the maximum and minimum obtained values. The cells produced from a single epi-structure presented a high reproducibility in performance, with the thin-film devices showing a slightly larger spread of the parameters due to the increased number and less routinely applied processing steps. Overall, the short-circuit current of the thin-film solar cells is higher than the equivalent substrate-based devices due to the reflectance at the rear mirror of the long wavelength portion of the incident light that is not absorbed in the first pass through the active layers. Furthermore, the relatively large front grid coverage (16.6%) causes the solar cells J_{sc}, and efficiency (η), to be proportionally reduced, as compared to previously reported cells [25,33]. If the J_{sc} is corrected for the active area, the devices' approximated average efficiencies range from 24.6% (thin SB-DJ) to 27% (TF-DJ). These efficiencies indicate high material quality, for which the BOL collection and mobility parameters are well approximated by the theoretical models [28,34].

The BOL dark saturation current densities J_{01} and J_{02} are deduced from the best fit of equation (1) to the cells dark characteristics and $J_{sc}-V_{oc}$ data under different light intensities. The extracted values are displayed in Table 1, together with all the relevant calculated BOL parameters for the five solar cell structures. The reason for the differences in minority carrier mobility values between the shallow and deep junction cells is due to the doping dependence of the diffusion coefficient [34] and the fact that the two geometries have different doping concentration of the emitter and base layers.

If S_p and S_n are assumed to be negligible, the calculated J_{01} values show a considerable discrepancy to the experimentally deduced values. From this, it could be deduced that, for all cells the interface recombination is limiting the dark curves at the $1kT$ region, with values ranging between 1×10^3 and 5×10^3 cm/s. With the analysis of the cells' EQE curves, S_p and S_n can be more precisely determined, and the resulting recombination velocities are depicted in Table 1.

3.2. Solar cell performance degradation upon proton irradiation

The averaged remaining factors of the illuminated $J-V$ parameters of the cells upon proton irradiation, normalized to the BOL values, are shown in Fig. 4, together with the modeled curves. It is clear that both thin-film and substrate based devices with a SJ geometry are less

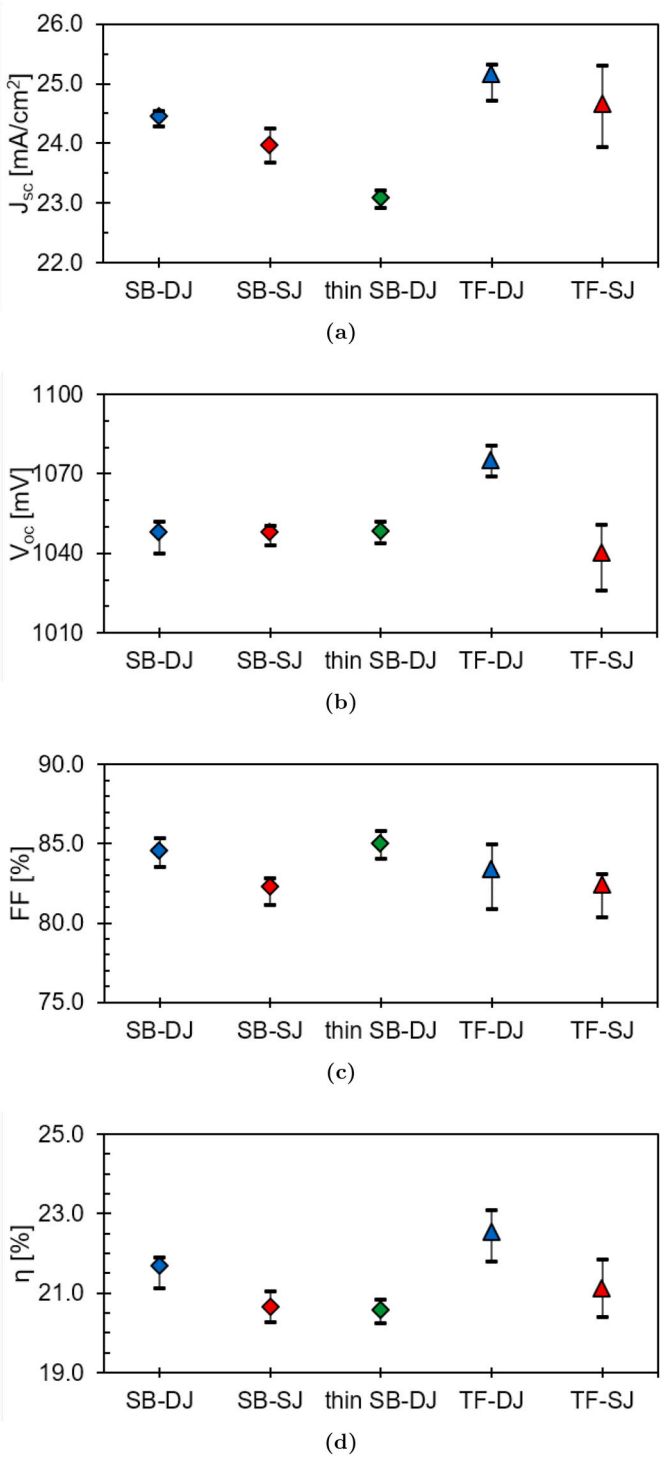

Fig. 3. Average, maximum and minimum experimentally determined values of the a) J_{sc}, b) V_{oc}, c) FF and d) η of the five studied architectures at the beginning of life.

sensitive to irradiation damage than the cells with the DJ geometry, and the thinner DJ cells present a much lower degradation than their thicker counterparts, in particular for lower fluences.

The J_{sc} and V_{oc} remaining factors overlap for both thin-film and substrate-based devices with similar junction depth, even though the absolute values are different due to the higher BOL performance of the TF cells, indicating that there is no additional Cu-related defects caused by the incidence of protons. This indicates that the use of copper foil as a convenient low-cost carrier and rear contact for thin-film solar cells does

Table 1
Fitted and calculated parameters from each solar cell structure at BOL.

Parameter	SB-DJ	SB-SJ	TF-DJ	TF-SJ	thin SB-DJ
J_{01} [A/cm^2]	6.0×10^{-20}	7.0×10^{-20}	1.5×10^{-20}	5.0×10^{-20}	6.0×10^{-20}
J_{02} [A/cm^2]	6.0×10^{-12}	5.0×10^{-12}	1.0×10^{-11}	1.2×10^{-11}	6.0×10^{-12}
f_{PR}	0.78	0.78	0.95	0.95	0.67
μ_p [cm^2/Vs]	304	134	304	134	273
$\tau_{p,SRH}$ [ns]	1703	8.0	1703	8.0	1361
τ_p [ns]	133	1.8	492	4.7	46.0
L_p [μm]	10.2	0.8	19.6	1.3	5.7
μ_n [cm^2/Vs]	2709	5554	2709	5554	2709
$\tau_{n,SRH}$ [ns]	9.9	283	9.9	283	9.9
τ_n [ns]	4.2	130	7.7	227	3.2
L_n [μm]	5.4	43.2	7.4	57.1	4.7
S_p [cm/s]	2.0×10^3	1.0×10^3	1.0×10^3	1.0×10^3	4.0×10^3
S_n [cm/s]	5.0×10^3	1.0×10^3	2.0×10^3	1.0×10^3	2.0×10^3

not require reconsideration because of the encountered proton irradiation in space applications.

Because proton irradiation exposure is expected to create uniform damage throughout the GaAs active layers, the radiation-related degradation is expected to be material dependent, creating displacement defects and reducing the average minority carriers lifetime. All changes in performance should, therefore, be caused primarily by reduction of the minority carriers lifetime and degradation of hetero-interfaces [22], being independent of solar cell geometry and processing steps. Because of this, the changes in dark $J-V$ and EQE characteristics of the thin-film cells upon irradiation are highly similar to those of the substrate-based cells, and therefore only the latter are shown in Figs. 5 and 6.

The performance degradation mechanism is well illustrated by the EQE curves, shown in Fig. 5. The differences between the SJ and DJ geometries are related to the fact that the absorption of light into the cell decreases exponentially, so the largest fraction of light is absorbed in the upper part of the cell. In the SJ cells (Fig. 5a), most of the photo-generated free carriers, therefore, only have to diffuse over a short distance to the $p-n$ junction to be drifted towards the right electrode and be collected. For longer wavelengths a smaller fraction of the light is able to penetrate deeper into the cell and consequently generate some minority carriers deeper in the base, which have to travel further before reaching the $p-n$ junction. Upon irradiation, these carriers face an increased SRH recombination probability, decreasing the EQE at longer wavelengths. In DJ cells (Fig. 5b), on the other hand, most of the minority carriers generated in the thick emitter have to diffuse over a long distance before reaching the $p-n$ junction, with the exception of the small fraction generated deeper in the cell. Therefore, the collection efficiency in these cells is basically reduced over the entire wavelength, being only slightly higher for the longer wavelength portion of the light.

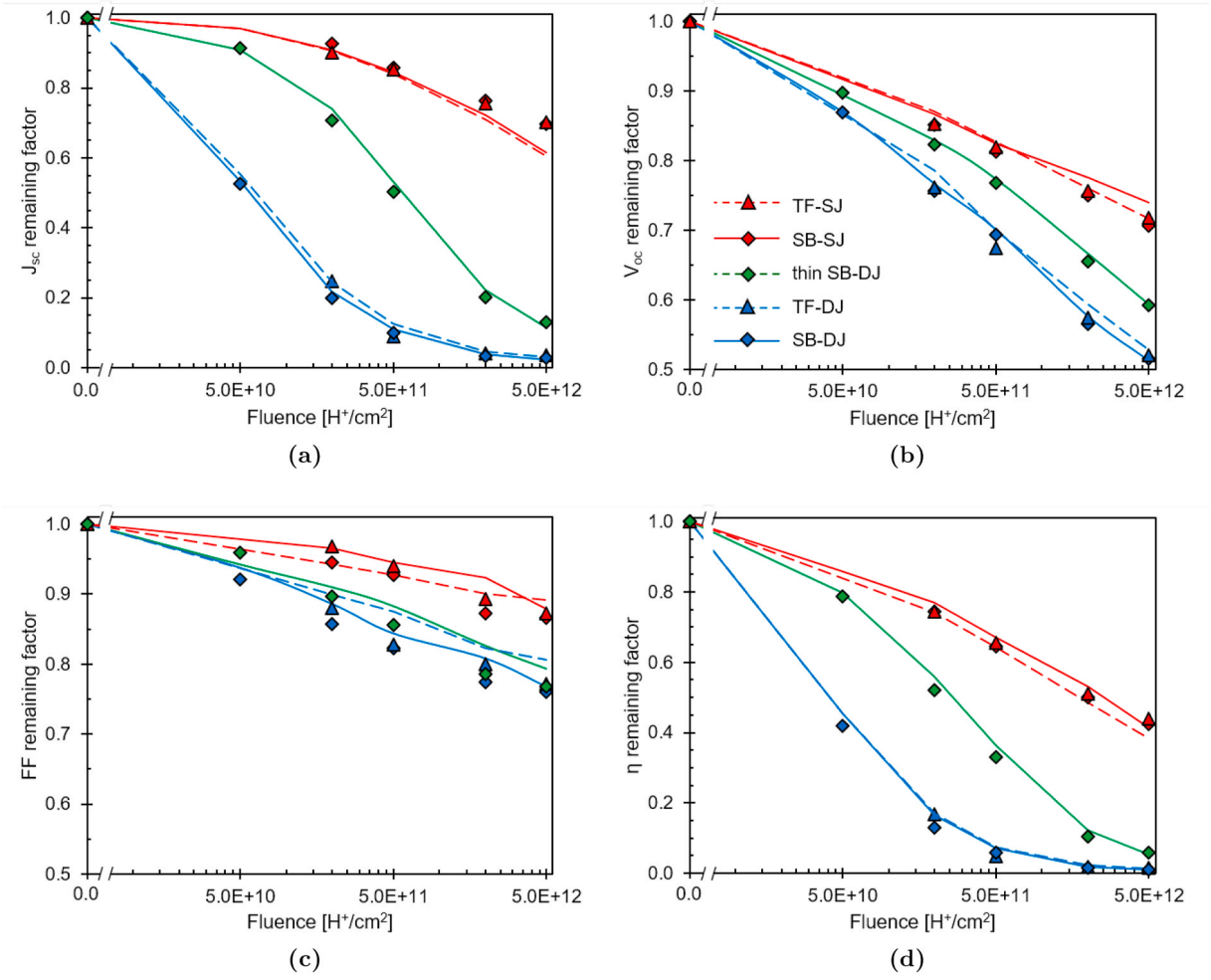

Fig. 4. Average remaining factors of a) J_{sc}, b) V_{oc}, c) FF and d) η of the four different structures subjected to different radiation doses. The markers in these figures represent the experimental results and the lines are the modeled curves.

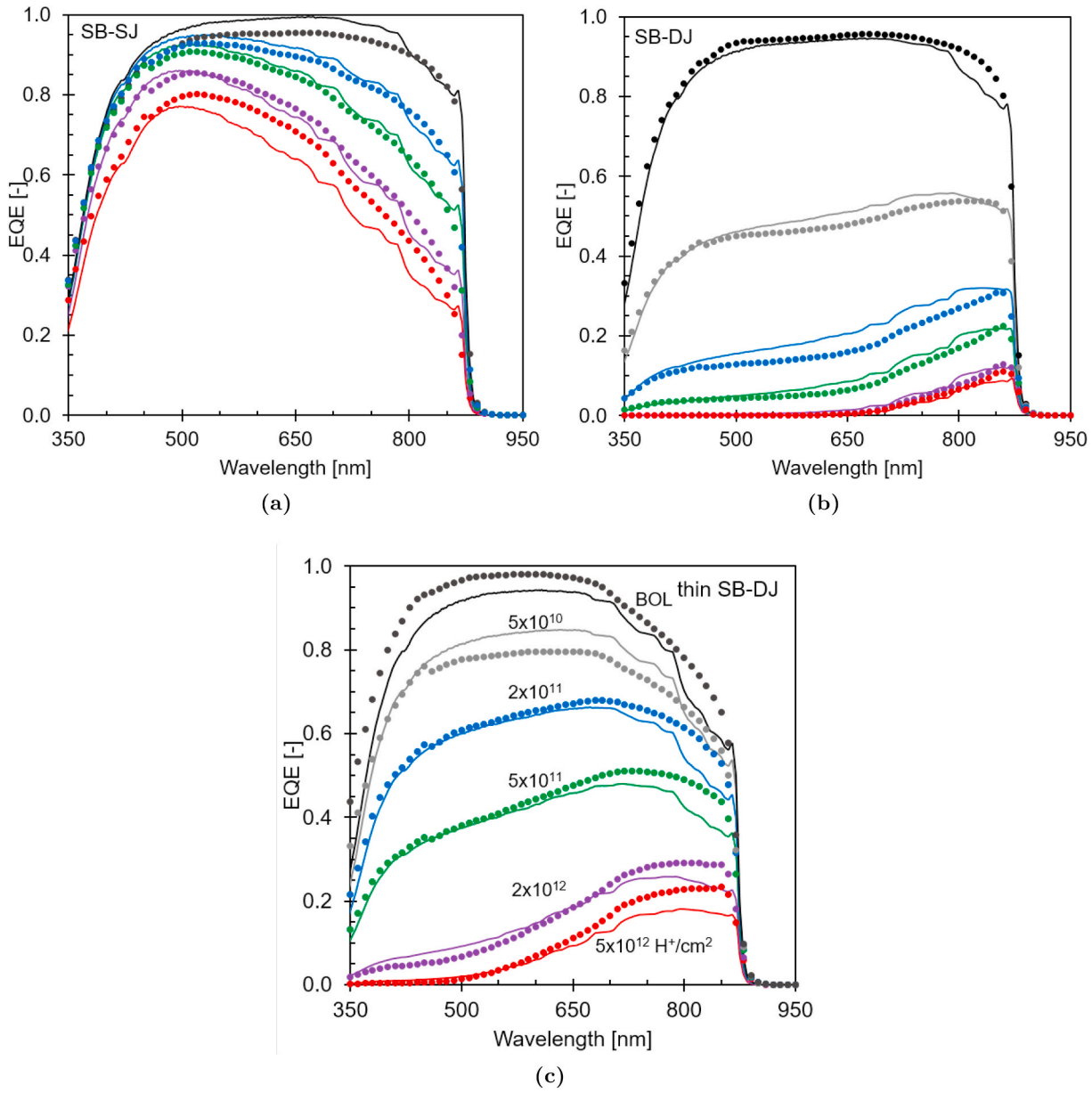

Fig. 5. External quantum efficiency curves of a) the shallow junction, b) the deep junction and c) the thinner deep junction solar cells in the substrate-based architecture after exposure to different doses of proton radiation. The markers represent the experimental results and the lines are the modeled curves.

The degradation of the thinner SB-DJ cells (Fig. 5c) has a similar profile, but the reduced emitter thickness results in a smaller average distance between the location where light is absorbed and the SCR, and therefore the reduction of the EQE is less extreme than for the thicker devices.

In Fig. 6 the measured dark curves (dark blue lines of connected markers) and the $J_{sc} - V_{oc}$ values under different illumination intensities (red markers) are shown, as well as the best 2-diode model fits (equation (1)) to these measured quantities. The extracted parameters J_{01} and J_{02} of the irradiated cells are displayed in Fig. 7. It is important to note that, in particular for the DJ solar cells, there may be some uncertainty with regards to the J_{01} values of the irradiated cells, since the dark curves are dominated by the $2kT$ component. The J_{01} increase for the different cell geometries is consistent with the degradation in EQE as described above, with a large difference between the saturation currents of the SJ and the DJ cells. The increase of J_{02}, on the other hand, is much more uniform between the solar cell architectures. This illustrates that, while the radiation-induced degradation of the perimeter and SCR affects the different cell geometries in a similar way, the junction depth determines how strongly the QNR and hetero-interfaces degradation will reduce the performance.

The total damage that the incidence of charged particles will generate in the semiconductor material is proportional to the incident particle non-ionizing energy loss (NIEL) [35,36], or the amount of energy deposited by the particle passing through the material and resulting in displacement processes. It is possible to calculate the absorbed NIEL dose (or the displacement damage dose, DDD) of different types of irradiation by:

$$DDD = \varphi \times \text{NIEL}, \tag{2}$$

where φ is the charged particle fluence. The NIEL values calculated by Baur et al. [36] for a displacement threshold energy of 21 eV, are $\text{NIEL}_e = 1.125 \times 10^{-5}$ MeVcm^2/g for 1-MeV electrons and $\text{NIEL}_p = 4.967 \times 10^{-2}$ MeVcm^2/g for 1-MeV protons. Using equation (2), the J_{sc} of the studied solar cells is presented as a function of DDD in Fig. 8. For comparison, the data from previously reported GaAs solar cells subjected to electron irradiation [22] is also presented in this figure.

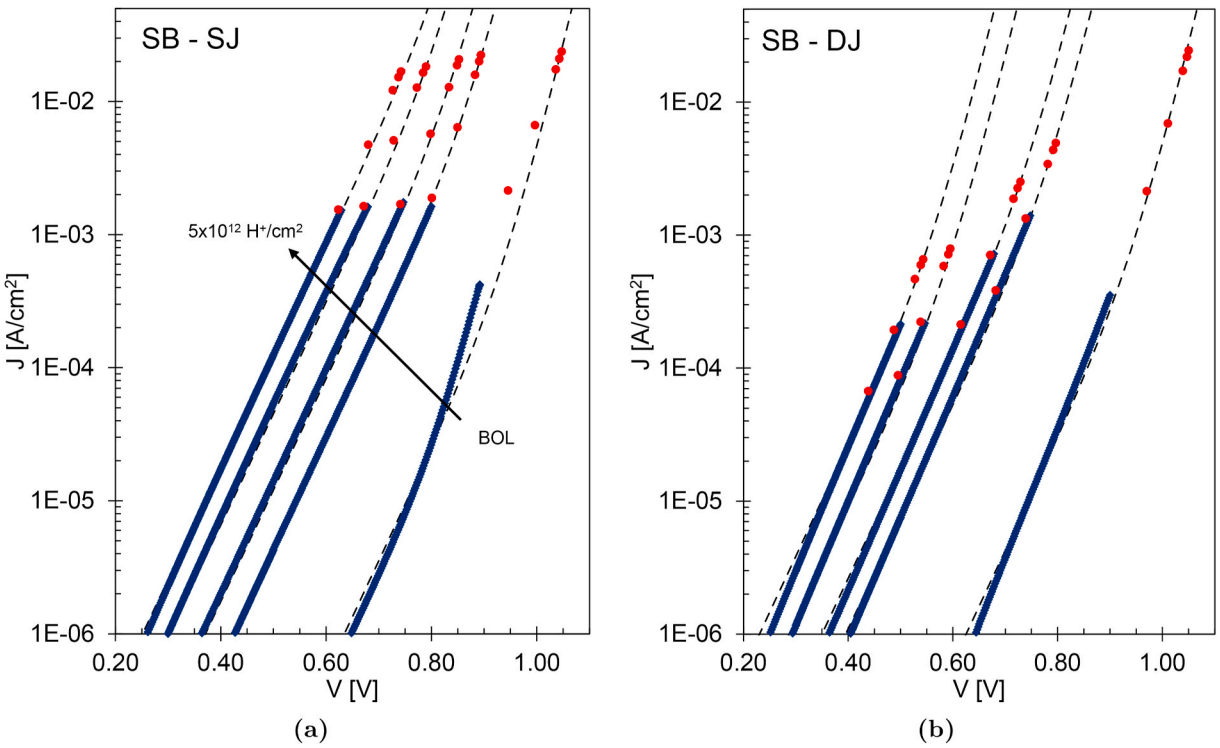

Fig. 6. Dark $J - V$ characteristics of a) shallow junction and b) deep junction solar cells in the substrate-based architecture after exposure to different levels of proton radiation. The isolated red circular markers represent the measured $J_{sc} - V_{oc}$ values under different light intensities, the square blue markers that appear as continuous lines are the measured dark curves and the dashed lines show the curves deduced from the 2-diode model (equation (1)). (For interpretation of the references to colour in this figure legend, the reader is referred to the Web version of this article.)

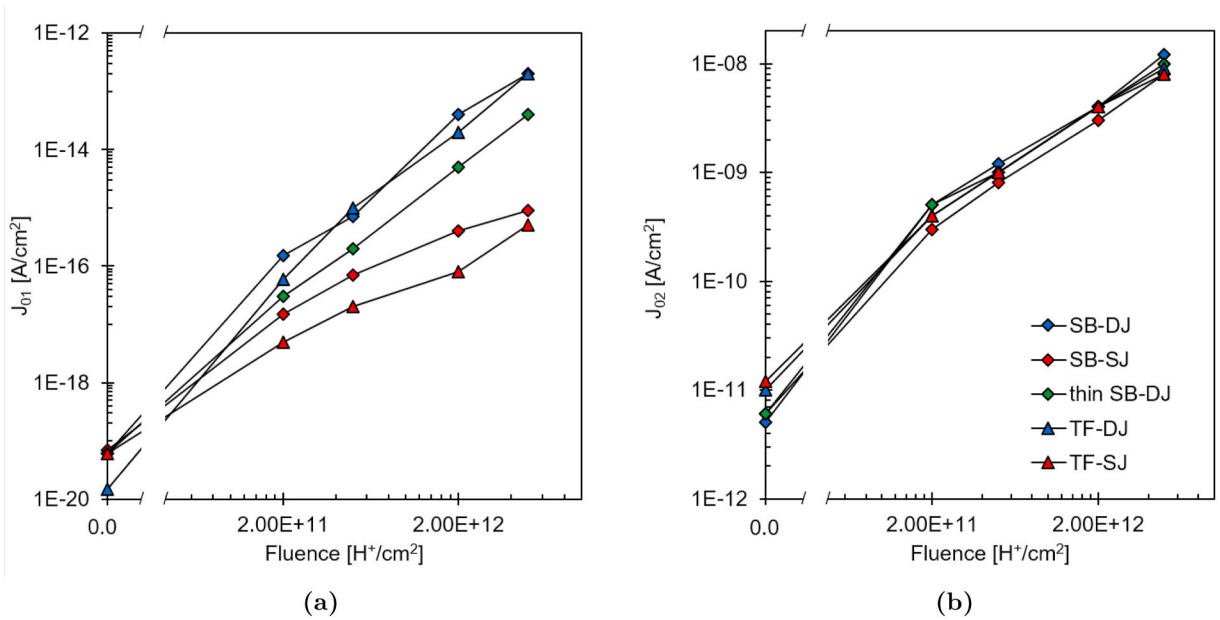

Fig. 7. Dark curve parameters a) J_{01} and b) J_{02} extracted from the dark curves of the solar cells subjected to different doses of proton irradiation, using the two-diode model (equation (1)). The lines in these figures are merely a guide to the eye.

Furthermore, the DDD value equivalent to the electron radiation dose of 1×10^{15} e^-/cm^2, usually associated to GEO missions, is highlighted by the dotted line in the figure as a reference.

Although the active layer thickness of the various cell configurations evaluated in the previous study were slightly different, overall the J_{sc} remaining factors from the proton and electron irradiated cells as a function of DDD show a good correlation. For the SJ cells, the small variations in thickness between the different studied cell structures do not impact the degradation, resulting in a near perfect overlap of results in the DDD range that is covered by each of the two irradiation studies. For the DJ cells, on the other hand, the degradation is very sensitive to the small changes in active layer thickness, resulting in small discontinuities between the curves following from e^- and H^+ irradiation. For the thinner DJ cells, the reason for the increased resilience to irradiation of

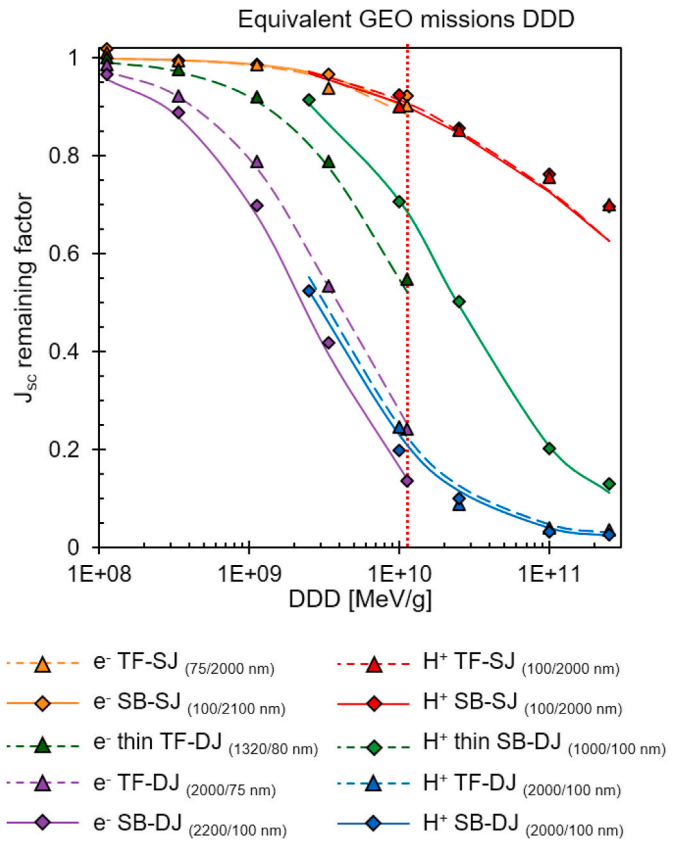

Fig. 8. J_{sc} remaining factor of the proton irradiated solar cells in this study as well as previously reported electron irradiated cells [22] related to the total displacement damage dose (DDD). The markers represent the experimental results and the lines are the modeled curves. The red vertical line indicates the equivalent DDD associated to GEO missions. (For interpretation of the references to colour in this figure legend, the reader is referred to the Web version of this article.)

the H^+ irradiated thin SB-DJ cells as compared to the e^- irradiated thin TF-DJ cells is due to the 300 nm difference in active layer thickness.

In order to simulate the cell performance upon proton irradiation, the decrease of the SRH lifetime $\tau_{p(n)_{SRH}}$ with proton fluence is modeled as:

$$\frac{1}{\tau_{p(n)_{SRH}}} = \frac{1}{\tau_{p(n)_{SRH,0}}} + K^p_{\tau_{p(n)}}\varphi_p, \tag{3}$$

where $\tau_{p(n)_{SRH,0}}$ is the SRH lifetime at BOL and $K^p_{\tau_{p(n)}}$ is the minority carrier lifetime damage constant for proton irradiation. Based on the results from a previous study [22], an increase of the surface recombination velocity at the window and BSF hetero-interfaces is also considered. For this purpose, $S_{p(n)}$ is expressed as:

$$S_{p(n)} = S_{p(n)_0} + K^p_{S_{p(n)}}\varphi_p, \tag{4}$$

where $S_{p(n)_0}$ is the value of $S_{p(n)}$ at BOL and $K_{S_{p(n)}}$ is the interface damage rate for proton irradiation. The lifetime degradation constants encountered in the previous study for electron irradiated GaAs cells are $K^e_{\tau_p} = 8.75 \times 10^{-7}$ cm^2/s and $K^e_{\tau_n} = 5.25 \times 10^{-6}$ cm^2/s. Because both $1/\tau_{p(n)}$ and $S_{p(n)}$ scale linearly with φ, which is also directly proportional to the DDD, it can be assumed that, for a certain DDD, electrons and protons cause similar degradation to the minority carrier lifetimes. Therefore, an approach was taken in which:

$$K^p_{\tau_{p(n)}} = K^e_{\tau_{p(n)}}\frac{NIEL_p}{NIEL_e}. \tag{5}$$

The $K^p_{\tau_{p(n)}}$ values used for fitting the experimentally obtained EQE and dark $J-V$ characteristics upon proton irradiation are the direct results from the equivalence proposed in equation (5). As a starting point, a similar conversion was made to $K^p_{S_{p(n)}}$, but since this latter value was found to vary between the different geometries of the electron irradiated cells [22], it was adjusted to improve the fitting of the curves. The resulting lifetime and interface recombination degradation constants used in the model are stated in Table 2.

Fig. 9 depicts the reciprocal lifetime values of the SB-DJ and SB-SJ cell geometries simulated using these constants, for a large range of DDD, equivalent to proton fluences from approximately 2×10^8 to 2×10^{13} H^+/cm^2. The equivalent DDD of the studied proton and electron [22] irradiation doses are marked. For high irradiation doses, the cells' minority carrier lifetime are limited by the $K_\tau\varphi$ component from equation (3), which is also highlighted in the figures, independent of their BOL values.

Aside from J_{sc} and V_{oc} degradation, the fill factor (FF) of the solar cells also decreases upon irradiation (see Fig. 4c). The shape of the illuminated $J-V$ curves of the irradiated cells presents an effect resembling that of a reduced shunt resistance (see example in Fig. 10b), yet the dark characteristics of the cells, shown in Fig. 6, do not indicate the same effect. This difference between the illuminated and dark characteristics was also observed in a study by Salzberger et al. [11], where the voltage dependency of the space charge region width is suggested to explain the voltage-dependent photo-current. We can model the width of the emitter (w_E) and base (w_B) fractions of the space charge region by Ref. [37]:

$$w_E = \sqrt{\frac{2\varepsilon_r\varepsilon_0}{q}\frac{N_A}{N_D(N_A+N_D)}(V_{bi}-V)} \tag{6}$$

and

$$w_B = \sqrt{\frac{2\varepsilon_r\varepsilon_0}{q}\frac{N_D}{N_A(N_A+N_D)}(V_{bi}-V)}$$

where ε_0 is the vacuum permittivity, ε_r is the relative permittivity of GaAs and V_{bi} is the built in potential of the junction. The proportions to which w_E and w_B are reduced upon the application of a voltage larger than zero, for the DJ and SJ geometries, are visualized in Fig. 10a. The effect of this reduction on the shape of the curve is illustrated in Fig. 10b, where the illuminated $J-V$ curve of an irradiated SB-DJ cell is simulated considering either a constant SCR width, equal to the width at $V = 0$ (dashed black line), or a V-dependent SCR width, calculated according to equations (6a) and (6b) (solid red line).

Because $L_{p(n)} \gg d_{E(B)}$ at BOL, the voltage-dependency of the SCR width does not affect the illuminated curves. After irradiation, however, the diffusion length is reduced so that $L_{p(n)} + w_{E(B)}$ is much smaller than the total layer thickness, and the collection of photo-generated carriers is directly affected by the reduction of SCR. This results in a decrease in the slope of the illuminated $J-V$ curve, similar to the effect of a reduced shunt resistance, and consequently, in a reduction of the FF. As in SJ

Table 2
Proton radiation induced damage constants, as deduced from the analysis of the $J-V$ and EQE measurements.

Solar cell geometry	Damage rates			
	K_{τ_p} [cm^2/s]	K_{τ_n} [cm^2/s]	K_{S_p} [cm^3/s]	K_{S_n} [cm^3/s]
SB-DJ	3.9×10^{-3}	2.3×10^{-2}	5×10^{-7}	4×10^{-7}
SB-SJ	3.9×10^{-3}	2.3×10^{-2}	5×10^{-9}	4×10^{-7}
TF-DJ	3.9×10^{-3}	2.3×10^{-2}	5×10^{-7}	4×10^{-7}
TF-SJ	3.9×10^{-3}	2.3×10^{-2}	5×10^{-9}	4×10^{-7}
thin SB-DJ	3.9×10^{-3}	2.3×10^{-2}	5×10^{-8}	4×10^{-7}

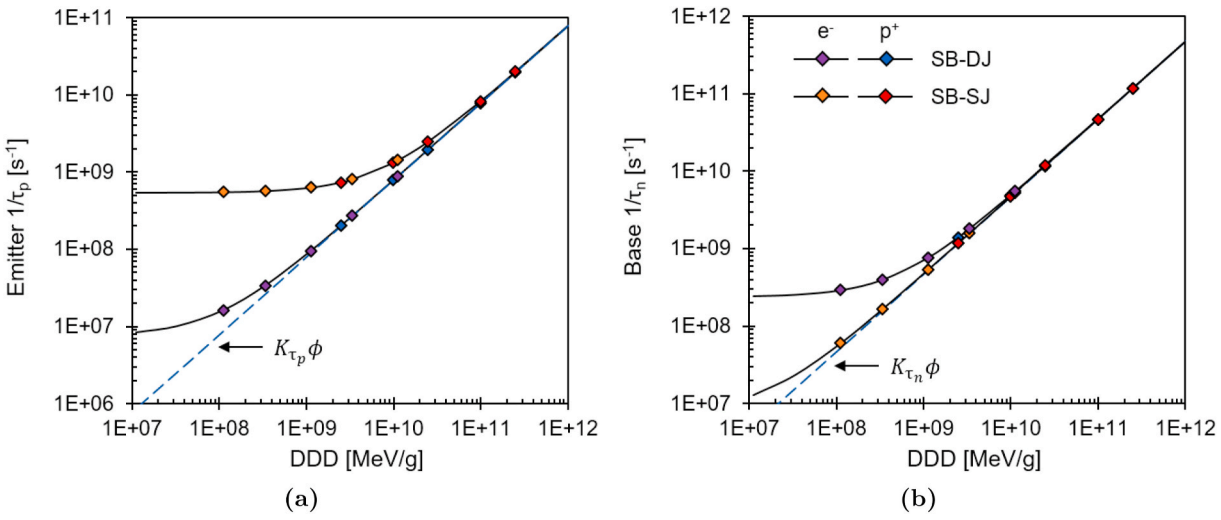

Fig. 9. Modeled a) emitter and b) base reciprocal minority carrier lifetimes of the SB-SJ and SB-DJ solar cells as a function of the displacement damage dose (DDD). The markers represent the equivalent DDD to the studied proton and electron irradiation doses of the present work and a previous study [22], respectively.

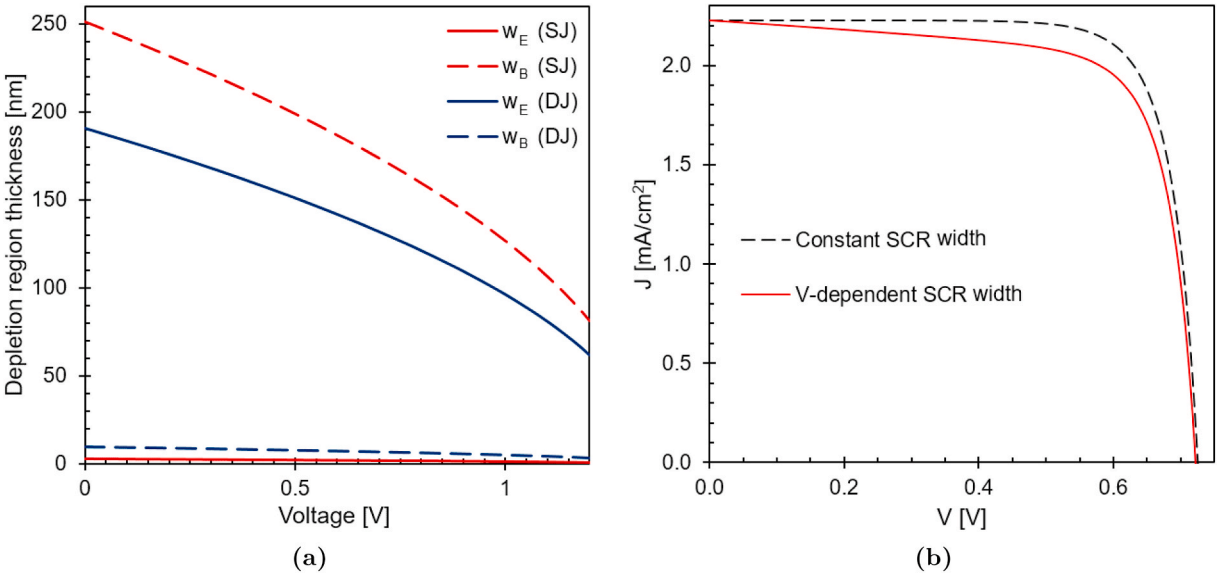

Fig. 10. a)Modeled emitter and base space charge region width as a function of the voltage for the SJ and DJ cell geometries. b) Example of two model simulations of $J - V$ curves, considering either a constant SCR width equal to the width for V = 0 (dashed black line) or a voltage-dependent SCR width (solid red line). (For interpretation of the references to colour in this figure legend, the reader is referred to the Web version of this article.)

devices the reduced SCR width affects more strongly the bottom portion of the cells, which has a lower carrier generation rate, the effect of proton irradiation on the FF of cells with this geometry is smaller.

The good agreement between the model simulations and the experimental curves, shown in Figs. 4, 5 and 8, further validates the previously developed CPS model to proton irradiation. The damage constants to the SRH lifetimes used in this study were directly converted from the previously extracted to electron irradiation, and minor adjustments were made to the interface recombination velocity damage constants. The present study clearly demonstrates that these constants can be converted and applied to predict cell performance degradation under proton irradiation, which suggests that the approach can probably be used to any particle type and energy with a known NIEL value. The performance degradation of a multitude of solar cell structures can therefore be simulated to the specific application conditions, providing a good quality of the epilayers at BOL.

4. Conclusions

In this study, a recently developed method to simulate the performance degradation of GaAs solar cells upon electron irradiation is applied to analyze the effects of proton irradiation exposure to the devices. In order to isolate the radiation damage to the bulk of the absorber from effects in the hetero-interfaces, solar cells with a broad range of architectures were subjected to proton irradiation fluences up to 5×10^{12} H^+/cm^2.

The reported degradation of the quality of the hetero-interfaces, characterized by an increase in interface recombination velocities, is also observed in this study. Furthermore, a NIEL-based conversion of the minority carrier lifetime as well as the interface recombination velocity degradation constants derived from the electron irradiation studies is sufficient to obtain a good correlation between experimental and theoretical results, further confirming the validity of the model. These degradation constants are material dependent, being quite insensitive to the cell's geometry and processing steps, allowing performance

prediction of GaAs solar cells of different architectures, not limited to the structures used in this study.

Because the utilized fluences are representative of more extreme radiation doses than the equivalent for GEO missions, a strong degradation in performance of all solar cell geometries is observed. It is shown that, similarly to electron irradiation, the incidence of protons affects the performance of the solar cells mainly by reducing the minority carrier lifetimes. Therefore, the distance from the space charge region to the location where carriers are generated is the determining aspect with regard to the cell's resilience to radiation. Since for the DJ cells upon irradiation the hole diffusion length is much smaller than the emitter thickness, the collection of generated carriers is strongly reduced, and this geometry presents a much larger decrease of J_{sc} as compared to SJ devices. Furthermore, a pronounced voltage dependency of the photocurrent is introduced in all cell structures, reducing the cells fill factor by up to 20%.

The main advantage of the thin-film geometry, as compared to substrate-based devices, is that the presence of a rear reflector allows the production of thinner cells with comparable efficiency. Thinner devices are less sensitive to reduced diffusion length, resulting in higher resilience to radiation damage. High quality thin-film solar cells also have the potential to achieve higher performances at beginning-of-life due to increased photon recycling, representing an interesting geometry for space applications. Copper foil represents a convenient low-cost carrier and rear contact for the such thin-film cells. Whereas copper diffusion can be a potential problem in semiconductor devices, the present study demonstrates that proton irradiation levels up to 5×10^{12} H^+/cm^2 do not induce such problems.

CRediT authorship contribution statement

Natasha Gruginskie: Formal analysis, Investigation, Writing - original draft, Visualization. **Federica Cappelluti:** Software, Methodology, Validation, Project administration. **Maarten van Eerden:** Investigation. **Gerard Bauhuis:** Resources, Investigation. **Peter Mulder:** Resources, Investigation. **Elias Vlieg:** Supervision. **John Schermer:** Conceptualization, Writing - review & editing, Project administration, Funding acquisition.

Declaration of competing interest

The authors declare that they have no known competing financial interests or personal relationships that could have appeared to influence the work reported in this paper.

Acknowledgements

The authors acknowledge financial support from the Brazilian National Council for Scientific and Technological Development, under the program Science Without Border, project 233259/2014-7, from the European Union's Horizon 2020 research and innovation program, under grant agreement 687253 TFQD (http://tfqd.eu), and funding under grant agreement 17043 REGENERATION from the European Institute for Innovation and Technology (EIT), a body supported by the European Union's Horizon 2020 research and innovation program.

References

[1] C.L. Stender, J. Adams, V. Elarde, T. Major, H. Miyamoto, M. Osowski, N. Pan, R. Tatavarti, F. Tuminello, A. Wibowo, C. Youtsey, G. Ragunathan, Flexible and lightweight epitaxial lift-off GaAs multi-junction solar cells for portable power and UAV applications, 2015 IEEE 42nd Photovoltaic Specialist Conference, PVSC 2015 (2015) 8, https://doi.org/10.1109/PVSC.2015.7356137.

[2] J. Feenstra, R.H.V. Leest, N.J. Smeenk, G. Oomen, E. Bongers, P. Mulder, E. Vlieg, J.J. Schermer, Flexible shielding layers for solar cells in space applications, J. Appl. Polym. Sci. (2016) 43661doi, https://doi.org/10.1002/app.43661.

[3] S. Moon, K. Kim, Y. Kim, J. Heo, J. Lee, Highly efficient single-junction GaAs thin-film solar cell on flexible substrate, Sci. Rep. 6 (February) (2016) 1–6, https://doi.org/10.1038/srep30107.

[4] P. Kwak, N. Kim, J. Kim, D. Kim, K. Song, J. Lee, Flexible space solar cell array with radiation shield fabricated by guided-printing of cover glasses, Sol. Energy Mater. Sol. Cell. 169 (2017) 210–214, https://doi.org/10.1016/j.solmat.2017.05.019. April.

[5] M.M.A.J. Voncken, J.J. Schermer, G.J. Bauhuis, P. Mulder, P.K. Larsen, Multiple release layer study of the intrinsic lateral etch rate of the epitaxial lift-off process, Appl. Phys. Mater. Sci. Process 79 (7) (2004) 1801–1807, https://doi.org/10.1007/s00339-003-2100-1.

[6] G.J. Bauhuis, P. Mulder, E.J. Haverkamp, J.J. Schermer, E. Bongers, G. Oomen, W. Köstler, G. Strobl, Wafer reuse for repeated growth of III-V solar cells, Prog. Photovoltaics Res. Appl. 18 (3) (2010) 155–159, https://doi.org/10.1002/pip.930.

[7] J. Adams, V. Elarde, A. Hains, C. Stender, F. Tuminello, C. Youtsey, A. Wibowo, M. Osowski, Demonstration of multiple substrate reuses for inverted metamorphic solar cells, in: 2012 IEEE 38th Photovoltaic Specialists Conference (PVSC) PART, vol. 2, 2012, pp. 1–6, https://doi.org/10.1109/PVSC-Vol2.2012.6656720.

[8] R.H. van Leest, K. de Kleijne, G.J. Bauhuis, P. Mulder, H. Cheun, H. Lee, W. Yoon, R. van der Heijden, E. Bongers, E. Vlieg, J.J. Schermer, Degradation mechanism(s) of GaAs solar cells with Cu contacts, Phys. Chem. Chem. Phys. 18 (15) (2016) 10232–10240, https://doi.org/10.1039/C6CP01428C. http://xlink.rsc.org/?DOI=C6CP01428C.

[9] R. Van Leest, P. Mulder, N. Gruginskie, S. Van Laar, G. Bauhuis, H. Cheun, H. Lee, W. Yoon, R. Van Der Heijden, E. Bongers, E. Vlieg, J. Schermer, Temperature-induced degradation of thin-film III-V solar cells for space applications, IEEE J. Photovoltaics 7 (2). doi:10.1109/JPHOTOV.2016.2642642..

[10] B.R. Elbert, Introduction to Satellite Comunication, Artech House, 2008, https://doi.org/10.1002/0470014008.

[11] M. Salzberger, M. Rutzinger, C. Nömayr, P. Lugli, C.G. Zimmermann, Voltage-dependent photocurrent in irradiated GaAs solar cells, September 2017, Prog. Photovoltaics Res. Appl. (2018) 1–7, https://doi.org/10.1002/pip.2983.

[12] J.C. Bourgoin, M. Zazoui, Irradiation-induced degradation in solar cell: characterization of recombination centres, Semicond. Sci. Technol. 17 (5) (2002) 453–460, https://doi.org/10.1088/0268-1242/17/5/308.

[13] J.H. Warner, S.R. Messenger, R.J. Walters, G.P. Summers, J.R. Lorentzen, D. M. Wilt, M.A. Smith, Correlation of electron radiation induced-damage in GaAs solar cells, IEEE Trans. Nucl. Sci. 53 (4) (2006) 1988–1994, https://doi.org/10.1109/TNS.2006.877877.

[14] L. Ming, W. Rong, Y. Kui, Y. Tiancheng, Photoluminescence analysis of electron irradiation-induced defects in GaAs/Ge space solar cells, Nucl. Instrum. Methods Phys. Res. Sect. B Beam Interact. Mater. Atoms 312 (2013) 137–140, https://doi.org/10.1016/j.nimb.2013.07.006.

[15] H. Mazouz, P.O. Logerais, A. Belghachi, O. Riou, F. Delaleux, J.F. Durastanti, Effect of electron irradiation fluence on the output parameters of GaAs solar cell, Int. J. Hydrogen Energy 40 (39) (2015) 13857–13865, https://doi.org/10.1016/j.ijhydene.2015.05.127.

[16] L. C. Hirst, M. K. Yakes, J. H. Warner, M. F. Bennett, K. J. Schmieder, R. J. Walters, P. P. Jenkins, Intrinsic radiation tolerance of ultra-thin GaAs solar cells, Appl. Phys. Lett. 109 (3). doi:10.1063/1.4959784.

[17] P. Dai, L. Ji, M. Tan, S. Uchida, Y. Wu, A. Abduwayiti, M. Heini, Q. Guo, L. Bian, S. Lu, H. Yang, Electron irradiation study of room-temperature wafer-bonded four-junction solar cell grown by MBE, Sol. Energy Mater. Sol. Cell. 171 (2017) 118–122, https://doi.org/10.1016/j.solmat.2017.06.046.

[18] A. Walker, S. Heckelmann, T. Tibbits, D. Lackner, A. Bett, F. Dimroth, Radiation hardness of AlGaAs n-i-p solar cells with higher bandgap intrinsic region, Sol. Energy Mater. Sol. Cell. 168 (2017) 234–240, https://doi.org/10.1016/j.solmat.2017.04.034.

[19] M. Yamaguchi, C. Amano, Numerical analysis for radiation-resistant GaAs heteroface solar cell structures, J. Appl. Phys. 57 (2) (1985) 537–544, https://doi.org/10.1063/1.334788.

[20] K. Bertness, B. Cavicchi, S. Kurtz, J. Olson, A. Kibbler, C. Kramer, Effect of base doping on radiation damage in GaAs single junction solar cells, Conference Record of the Twenty-Second IEEE Photovoltaic Specialists Conference, 2, 1991, pp. 1582–1587.

[21] C. Pellegrino, C.G. Zimmermann, Difference in space – charge recombination of proton and electron irradiated GaAs solar cells, Prog. Photovoltaics Res. Appl. 27 (2019) 379–390, https://doi.org/10.1002/pip.3100. November 2018.

[22] N. Gruginskie, F. Cappelluti, G. Bauhuis, P. Mulder, E. Haverkamp, E. Vlieg, J. Schermer, Electron radiation induced degradation of gaas solar cells with different architectures, Prog. Photovoltaics Res. Appl. 28 (2019) 266–278, https://doi.org/10.1002/pip.3224.

[23] B. E. Anspaugh, GaAs Solar Cell Radiation Handbook.

[24] R.H. Maurer, G.A. Herbert, J.D. Kinnison, A. Meulenberg, Gallium arsenide solar cell radiation damage study, IEEE Trans. Nucl. Sci. 36 (6) (1989) 2083–2091, https://doi.org/10.1109/23.45408.

[25] G. Bauhuis, P. Mulder, Y.Y. Hu, J. Schermer, Deep junction III-V solar cells with enhanced performance, Phys. Status Solidi (A) Appl. Mater. Sci. 213 (8) (2016) 2216–2222, https://doi.org/10.1002/pssa.201532903.

[26] M.P. Lumb, C.G. Bailey, J.G.J. Adams, G. Hillier, F. Tuminello, V.C. Elarde, R. J. Walters, Extending the 1-d hovel model for coherent and incoherent back reflections in homojunction solar cells, IEEE J. Quant. Electron. 49 (5) (2013) 462–470, https://doi.org/10.1109/JQE.2013.2252148.

[27] M. A. Steiner, J. F. Geisz, I. García, D. J. Friedman, A. Duda, S. R. Kurtz, Optical enhancement of the open-circuit voltage in high quality GaAs solar cells, J. Appl. Phys. 113 (123109). doi:10.1063/1.4798267..

[28] M. P. Lumb, M. A. Steiner, J. F. Geisz, R. J. Walters, Incorporating photon recycling into the analytical drift-diffusion model of high efficiency solar cells, J. Appl. Phys. 116 (19). doi:10.1063/1.4902320. URL https://doi.org/10.1063/1.4902320.
[29] H. Hovel, Semiconductors and semimetals. volume 11. Sol. Cell..
[30] C.-T. Sah, R.N. Noyce, W. Shockley, Carrier generation and recombination in P-N junctions, Proc. IRE 45 (9) (1957) 1243, https://doi.org/10.1109/JRPROC.1957.278528.
[31] M. Ochoa, C. Algora, P. Espinet-González, I. García, 3-D modeling of perimeter recombination in GaAs diodes and its in fl uence on concentrator solar cells, Sol. Energy Mater. Sol. Cell. 120 (2014) 48–58, https://doi.org/10.1016/j.solmat.2013.08.009.
[32] P. Espinet-González, I. Rey-Stolle, M. Ochoa, C. Algora, I. García, E. Barrigón, Analysis of perimeter recombination in the subcells of GaInP/GaAs/Ge triple-junction solar cells, Prog. Photovoltaics Res. Appl. 23 (2015) 874–882, https://doi.org/10.1002/pip.2501.
[33] G.J. Bauhuis, P. Mulder, E.J. Haverkamp, J.C.C.M. Huijben, J.J. Schermer, 26.1% thin-film GaAs solar cell using epitaxial lift-off, Sol. Energy Mater. Sol. Cell. 93 (9) (2009) 1488–1491, https://doi.org/10.1016/j.solmat.2009.03.027.
[34] M. Sotoodeh, A.H. Khalid, A.A. Rezazadeh, Empirical low-field mobility model for III-V compounds applicable in device simulation codes, J. Appl. Phys. 87 (6) (2000) 2890–2900, https://doi.org/10.1063/1.372274.
[35] S.R. Messenger, G.P. Summers, E.A. Burke, R.J. Walters, M.A. Xapsos, Modeling solar cell degradation in space: a comparison of the NRL displacement damage dose and the JPL equivalent fluence approaches, Prog. Photovoltaics Res. Appl. 9 (2001) 103–121, https://doi.org/10.1002/pip.357.
[36] C. Baur, M. Gervasi, P. Nieminen, S. Pensotti, P. G. Rancoita, M. Tacconi, NIEL Dose Dependence for Solar Cells Irradiated with Electrons and Protons.
[37] S.M. Sze, Physics of Semiconductor Devices, second ed., John Wiley and Sons, 1981.